

In vivo diffusion tensor imaging (DTI) of brain subdivisions and vocal pathways in songbirds

Geert De Groof,^{a,*} Marleen Verhoye,^{a,b} Vincent Van Meir,^a Ilse Tindemans,^a
Alexander Leemans,^b and Annemie Van der Linden^a

^aBio-Imaging Laboratory, University of Antwerp, CGB, Groenenborgerlaan 171, B-2020 Antwerp, Belgium

^bVision Laboratory, University of Antwerp, Belgium

Received 4 January 2005; revised 20 July 2005; accepted 7 September 2005
Available online 19 October 2005

The neural substrate for song behavior in songbirds, the song control system (SCS), is thus far the best-documented brain circuit in which to study neuroplasticity and adult neurogenesis. Not only does the volume of the key song control nuclei change in size, but also the density of the connections between them changes as a function of seasonal and hormonal influences. This study explores the potentials of in vivo Diffusion-Tensor MRI (DT-MRI or DTI) to visualize the distinct, concentrated connections of the SCS in the brain of the starling (*Sturnus vulgaris*). In vivo DTI on starling was performed on a 7T MR system using sagittal and coronal slices. DTI was accomplished with diffusion gradients applied in seven non-collinear directions. Fractional Anisotropy (FA)-maps allowed us to distinguish most of the grey matter and white matter-tracts, including the laminae subdividing the avian telencephalon and the tracts connecting the major song control nuclei (e.g., HVC with RA and X). The FA-maps also allowed us to discern a number of song control, auditory and visual nuclei. Fiber tracking was implemented to illustrate the discrimination of all tracts running from and to RA. Because of the remarkable plasticity inherent to the songbird brain, the successful implementation of DTI in this model could represent a useful tool for the in vivo exploration of fiber degeneration and regeneration and the biological mechanisms involved in brain plasticity.

© 2005 Elsevier Inc. All rights reserved.

Keywords: Imaging; Magnetic Resonance Imaging (MRI); Diffusion Tensor Imaging (DTI); Fiber-tracking; HVC; Robust nucleus of Arcopallium (RA); Starling (*Sturnus vulgaris*); Songbird brain; Bird

Introduction

The diffusion weighted image contrast in tissues is a well-accepted supplementary tool for tissue characterization. It is based on the restricted molecular movement of water within and

between cells. Using Diffusion Weighted-proton (H^+) MRI, moving proton spins will undergo a phase difference resulting in a signal intensity attenuation on MR-images (Stejskal and Tanner, 1965). In a sample where the barriers are not coherently oriented, diffusion is the same in all directions and is termed isotropic diffusion. However, if diffusion depends on direction, as in a sample with highly oriented barriers, it is termed anisotropic diffusion. In this way, structural subtypes can be identified simply based on their diffusion characteristics and the anisotropy is directly related to the geometry of the fibers. Moseley et al. (1990) confirmed that water diffusion in cat brain was anisotropic in normal white matter whereas diffusion was isotropic in grey matter. This was also confirmed for the human brain by Ahlhelm et al. (2004). The visualization of bundles of axons connecting distant brain regions (in vivo Fiber-tracking) is accomplished by measuring the diffusion tensor (using different images with diffusion weighting along non-collinear gradient axes) of the endogenous water along the axons (Mori and Barker, 1999). Diffusion Tensor Imaging (DTI) is therefore increasingly used for brain imaging in human studies. Recently, in vivo studies on small animals have been performed, although all studies thus far have been restricted to the mammalian brain, i.e., in rats (Xue et al., 1999; Lin et al., 2001), in mice (Xue et al., 1999; Lin et al., 2001; Zhang et al., 2002; Song et al., 2002, 2003, 2004; Sun et al., 2003) and in cats (Ronen et al., 2003; Kim et al., 2003).

There are strong indications that most functional sensory, motor and cognitive regions found in the mammalian telencephalon are also present in the avian telencephalon, although both animal groups display remarkable differences in telencephalic anatomy (Reiner et al., 2004; Jarvis et al., 2005). The telencephalon of birds consists of conglomerations of grey matter separated by thin lamina of white matter. This is in contrast to the cerebral organization in mammals, where a superficial thin layer of grey matter (the laminated cortex) is clearly separated from the underlying structure of grey matter (the basal ganglia) by a thick mass of myelinated axons, the internal capsule.

This mammalian brain anatomy has proved very accessible to conventional MRI methods (T_2 -, T_1 - or Proton Density-weighted

* Corresponding author. Fax: +32 3 265 32 33.

E-mail address: Geert.DeGroof@ua.ac.be (G. De Groof).

Available online on ScienceDirect (www.sciencedirect.com).

MRI), providing superior contrast differences between white and grey matter. As a result, interesting applications have appeared, such as morphometrical MRI measurements evaluating discrepancies in the distribution of grey and white matter between subjects with different behavioral backgrounds (e.g., taxi drivers or professional musicians (Maguire et al., 2000; Gaser and Schlaug, 2003)). Recently, DTI has contributed to these human studies by providing more detailed and 3D information on the white matter fiber tracts in the brain (Yamazaki et al., 2004). In contrast, the telencephalon of birds is quite different in its gross appearance from that of mammals and a clear morphometrical distinction between grey matter and myelinated axons cannot be made using conventional intrinsic MRI contrast settings, even at high resolution (Van der Linden et al., 1998; Verhoye et al., 1998). This lack of intrinsic contrast in avian brain tissue not only applies to the subtle laminae consisting of fibers dividing telencephalic brain regions, but also to inherent differences in cytoarchitecture and even to more obvious differences between specific nuclei, such as those delineating the song control system (SCS) of songbirds (Tramontin et al., 1998; Tramontin and Brenowitz, 2000; Thompson and Brenowitz, 2005). This system is responsible for the learning and production of learned complex vocalizations (song) and is the most well documented part of the songbird brain. It provides a unique and excellent model for the study of brain plasticity, learning and the neural substrate of an easily quantifiable behavior (song production). The telencephalic part of this system shows a remarkable sexual dimorphism in species with sexual dimorphism in song behavior (Del Negro and Edeline, 2001; Van der Linden et al., 2002; Riters and Ball, 2002; Thompson and Brenowitz, 2005) and a remarkable seasonal plasticity in species where song output changes with seasons (Ball et al., 2004; Brenowitz, 2004). Some parts of the circuit develop in a period during which the juvenile learns its songs from adult conspecific birds (Aamodt et al., 1992).

The non-invasive, in vivo nature of MRI renders it an exquisite tool with which to study brain plasticity, brain behavior interactions and associated phenomena. However, previous MRI studies on the song bird brain using T_2 - and Proton Density-weighted datasets (Van der Linden et al., 1998; Verhoye et al., 1998) failed to discern the song control nuclei and the fiber bundles that connect them. More recently, the use of an in vivo tract tracing technique based on the stereotaxic injection of paramagnetic Mn^{2+} in HVC, a key nucleus of the song control system (HVC is the name, not an abbreviation), allowed successful labeling of its two targets, namely the robust nucleus of the arcopallium (RA) and area X of the basal ganglia (Van der Linden et al., 2002, 2004; Tindemans et al., 2003), but still failed to show the fiber bundles that connect them. By adopting dynamic measurements, known as Dynamic Manganese enhanced (DME)-MRI, we evaluated the functional status of the song control circuit while birds were exposed to conspecific song (Tindemans et al., 2003) or under different endocrine conditions that changed the physiological status of the circuit (Van Meir et al., 2004). However, despite its advantages for analyzing functional changes in physiological status using repeated observations within individual subjects, the DME-MRI method has certain drawbacks. One of these is that the interpretation of changes in neuronal activity, which may come about as a result of the accumulation of Mn^{2+} in the target regions, is blurred by potential morphological changes in connectivity and cell density, especially if the measurements are performed over long time periods. Also, the ME-MRI technique is not completely non-

invasive and small brain lesions can still occur. DTI could therefore be a complementary non-invasive tool that quantifies the morphological changes in the song control system occurring during seasonal and endocrine changes.

This paper represents the first detailed evaluation of the application of DTI to the songbird brain and explores the potential of further applications in this model. Data will be discussed in the light of future technical developments in order to establish a quantitative technique that can be applied in this remarkable animal model exhibiting seasonal changes in song behavior with concomitant functional and morphological plasticity of the brain regions involved.

Materials and methods

Experimental setup

Twelve male starlings (*Sturnus vulgaris*; ± 75 g) were obtained from a stock maintained at the Drie Eiken Campus (UA, Antwerp) and housed in two indoor cages ($1.40 \times 2.20 \times 2.10$ m³) with imitated natural light–dark cycle for that time of year. The experiments were conducted between April 7 and April 26, 2004 during the breeding season in Belgium. All experimental procedures were approved by the Committee on Animal Care and Use at the University of Antwerp, Belgium.

DT-MRI protocol

The birds were anaesthetized as described previously (Van Meir et al., 2004) with an initial intramuscular (chest) injection of 5 ml/kg of a mixture containing 4.33 ml saline solution, 0.33 ml xylazine (Rompun: 20 mg/ml) and 2.10 ml ketamine (Ketalar: 50 mg/ml). During the whole experiment, the starlings were kept anaesthetized through an infusion of the mixture into the chest muscle at a constant rate of 0.15 ml/h. Body temperature was continuously monitored and kept within the range of 40–41°C.

A nonmagnetic Teflon™ stereotaxic beak-bar and head-holder combined with a radio frequency receiver surface antenna (diameter 24 mm) and a Helmholtz transmitter antenna (diameter 45 mm) fixed the bird's head position. Imaging was carried out on a 7 T horizontal bore MR microscope (MRRS, Guilford, UK), provided with shielded gradients (8 cm width, maximal strength = 400 mT/m; Magnex Scientific Ltd., Oxfordshire, UK). First, pilot

Table 1
The used diffusion gradient scheme

DW-image	G_{read}	G_{phase}	G_{slice}
1	0	0	0
2	1	1	0
3	1	−1	0
4	0	1	1
5	0	−1	1
6	1	0	1
7	−1	0	1

G_{read} , G_{phase} , G_{slice} code for the applied diffusion gradient in readout, phase encoding, and slice selection directions.

“1”, “−1” and “0” stand for the application of positive, negative and no diffusion gradients.

Table 2

Summary of key brain structures – comprising the song control system (SCS), the laminae, the visual and auditory system – visualized on the different maps and images

	(FE)FA-map	Trace map	RA map	Images
<i>SCS</i>				
Area X	•		•	6, 7
RA	•	•	•	2, 4, 5, 6, 7
HVC-to-RA tract	•		•	6, 7
HVC	•			7
MMAN	•	•	•	2, 3, 4, 5, 6, 7
LMAN	•		•	2, 3, 7
DLM	•	•	•	1, 4, 6
Hypoglossal nucleus	•		•	2, 3, 5, 6
<i>Laminae</i>				
LaM	•		•	2, 3, 7
LPS	•		•	2, 3, 7
LFS	•		•	2, 3, 7
<i>Visual</i>				
CO	•		•	1, 4, 5, 6, 7
Rt	•	•	•	2, 4, 5
<i>Auditory</i>				
Field L	•		•	1, 2, 4, 5, 7
MLD	•	•	•	1, 2, 4, 5, 6, 7
Ov	•		•	2, 4, 7

1, 2, 3, 4, 5, 6, 7 are the respective DW images with diffusion gradient directions shown in Table 1. Abbreviations: RA: robust nucleus of the arcopallium, MMAN: medial magnocellular nucleus of anterior nidopallium, LMAN: lateral magnocellular nucleus of anterior nidopallium, DLM: Nucleus dorsolateralis anterior thalami, pars medialis, LaM: lamina mesopallialis, LPS: lamina pallio-subpallialis, LFS: lamina frontalis superior, CO: chiasma opticum, Rt: nucleus Rotundus, MLD: nucleus mesencephalicus lateralis, pars dorsalis, Ov: nucleus ovoidalis.

images were acquired in three orthogonal directions. Secondly, DTI-MR data were obtained consisting of 24 sagittal slices (thickness 0.4 mm) covering one hemisphere of the starling brain ($n = 10$) or consisting of 18 coronal slices (thickness of 0.6 mm) covering the whole brain ($n = 2$). The orientation of the coronal images was selected to allow direct comparison of the DTI-data with the plates of the stereotaxic atlas of Stokes et al. (1974).

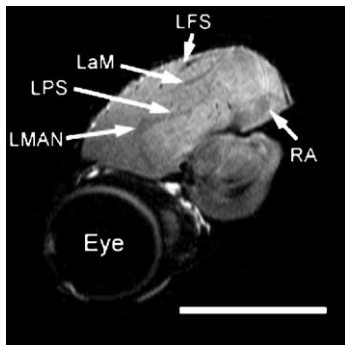


Fig. 1. Slice positioned 3.2 mm from the midsagittal plane from a set of images obtained applying diffusion gradients in the negative vertical (–read) and positive through-plane (+slice) direction (see Table 1: image 7). Abbreviations: LaM: lamina mesopallialis; LFS: lamina frontalis superior; LMAN: lateral magnocellular nucleus of anterior nidopallium; LPS: lamina pallio-subpallialis; RA: Robust nucleus of the arcopallium. Scale bar = 10 mm.

Diffusion Weighted (DW)-SE images were acquired with diffusion gradients applied in seven non-collinear directions (diffusion gradient strength = 69 mT/m for each direction, time diffusion gradient $\delta = 12$ ms, interval between onsets diffusion gradients $\Delta = 20$ ms) (Table 1).

Additional image parameters: field of view (FOV) = 25 mm (sagittal slices) and 28 mm (coronal slices), spectral width = 25 kHz, TE = 43 ms, TR = 2200 ms for sagittal slices and 2000 ms for coronal slices, acquisition matrix = 256 × 128 and 14 averages.

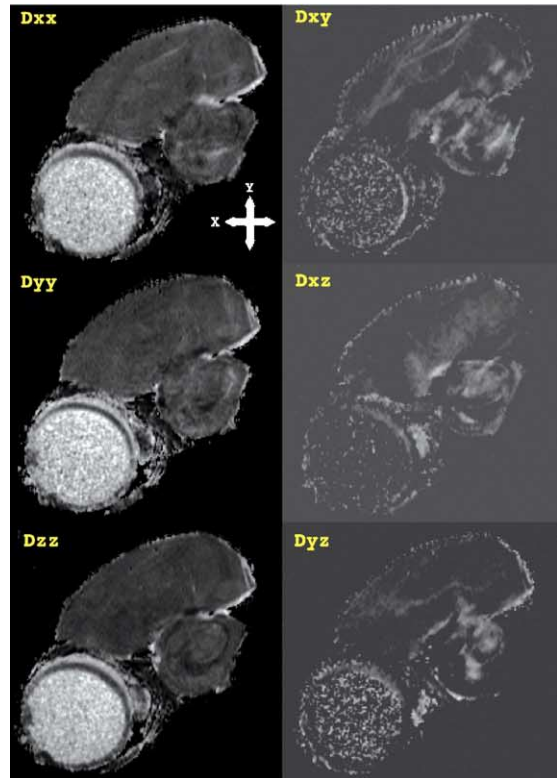
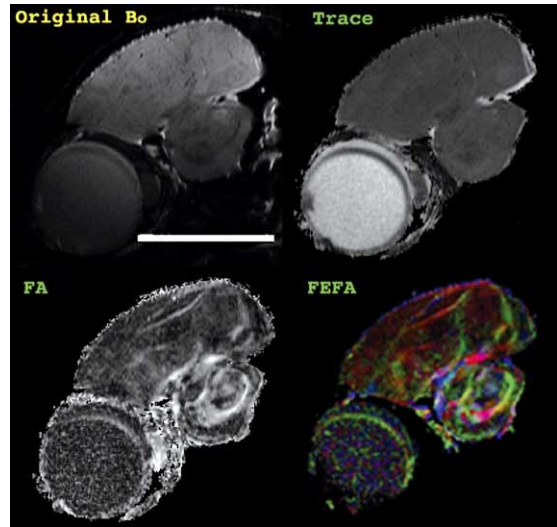


Fig. 2. Example of the different maps obtained from one DTI experiment of a slice taken 2.8 mm from midsagittal. Top-left: original non-DW-image. Top: Trace, FA: Fractional Anisotropy and FEFA: First Eigenvector Fractional Anisotropy-map. Bottom: (Dxx, Dxy, Dxz, Dyy, Dyz, Dzz): matrix of the individual tensor components of the slice. Scale bar = 10 mm.

Each DT-MRI experiment took approximately 8.5 h. All starlings recovered perfectly after the MR experiment.

DT-MRI data processing

The six DW-images were coregistered to the non-DW image (b_0 -image) by maximization of mutual information (MIRIT, Multimodality Image Registration using Information Theory) (Maes et al., 1997). The b matrices were calculated using analytical expressions (Mattiello et al., 1997) incorporating diffusion gradients and image gradients (b value (diffusion gradients only) = 788 s/mm²).

Diffusion tensor images and Fractional Anisotropy (FA)-maps were calculated using a MATLAB code (The Mathworks Inc., Natick, Massachusetts, USA). FA is a measure of the directionality of the water diffusion within a given voxel and is computed on a voxel-by-voxel basis using equation (Le Bihan et al., 2001):

$$FA = \frac{\sqrt{3[(\lambda_1 - \langle\lambda\rangle)^2 + (\lambda_2 - \langle\lambda\rangle)^2 + (\lambda_3 - \langle\lambda\rangle)^2]}}{\sqrt{2(\lambda_1^2 + \lambda_2^2 + \lambda_3^2)}}$$

with λ_1 , λ_2 , λ_3 the eigenvalues of the diffusion tensor and $\langle\lambda\rangle$ the average of the three eigenvalues.

Brain structures were assigned on FA-maps using the new nomenclature (Reiner et al., 2004). Additionally, first eigenvector fractional anisotropy (FEFA) maps were calculated in which the intensity reflects the FA-value and the color represents the orientation of the principal diffusion direction given by the first eigenvector (red = rostral ↔ caudal orientation, green = dorsal ↔ ventral orientation, blue = medial ↔ lateral orientation).

DTI fiber tracking

Fiber tracking was applied to the diffusion tensor data sets. A custom-written DTI fiber tracking tool has been developed and tested on synthetic diffusion tensor data (Leemans et al., 2005a,b). The fiber tracking algorithm is based on the FACT (fiber assignment by continuous tracking) approach (Mori et al., 1999). Here, 3D

tracking of axonal projections is performed on the continuous diffusion tensor field, which is calculated from the discrete raw diffusion tensor data. Fiber tracking is initiated from the center of a voxel and proceeds according to the local principal diffusion direction. At the point where the track enters the next voxel, its direction is changed to that of the new local neighborhood. Due to the presence of continuous intercepts, this tracking now connects the correct voxels and can assign the actual fiber pathway. Fiber tracking is stopped when the principal diffusion direction within a local neighborhood exceeds an incoherency threshold. The FA threshold for starting the tracking procedure was set to 0.43, the FA threshold for stopping the procedure was set to 0.087. The maximal curvature of the fibers was set to 0.8 and the step size was set to 1.0. The ROI for ‘seeding’ the tracking algorithm were chosen manually around the song nuclei RA (robust nucleus of the arcopallium). The color code of the fibers represents the orientation of the principal diffusion direction, by analogy with the FEFA-maps.

Results

Not every image or map provides the same information

Each single DTI experiment in this study generated 7 images and 10 maps. As can be seen in Table 2, each plain diffusion weighted image reveals different neuroanatomical structures depending on the applied diffusion directions. For example, the image set obtained according to image 7 diffusion directions (Table 1) reveals most of the song control nuclei, the different laminae and some auditory and visual nuclei (Fig. 1).

The six independent elements of the diffusion tensor are shown in 6 different tensor maps (Dxx, Dxy, Dxz, Dyy, Dyz, Dzz), as illustrated in Fig. 2. Here the diagonal elements (Dxx, Dyy, Dzz) indicate the molecular mobility in orthogonal directions, and the off-diagonal elements (Dxy, Dxz, Dyz) express how diffusion in one direction is correlated with displacement in a perpendicular direction. Because of the different function of the diagonal and off-diagonal tensor maps, they have a different contrast/brightness. Fig. 3 illustrates that every tensor element map shows a different contrast, by displaying the same anatomical slice but each time with a different calculated direction of diffusion (Dxx, Dyy and Dzz)

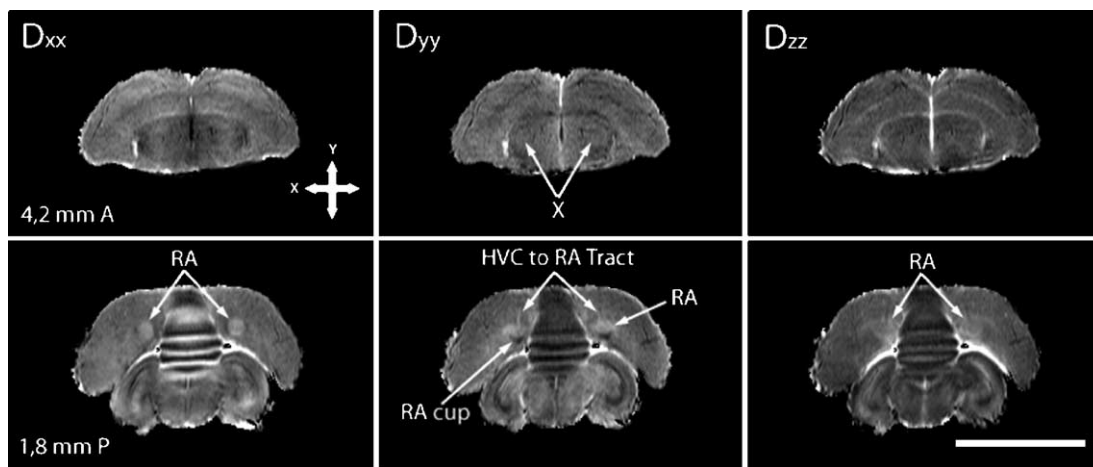
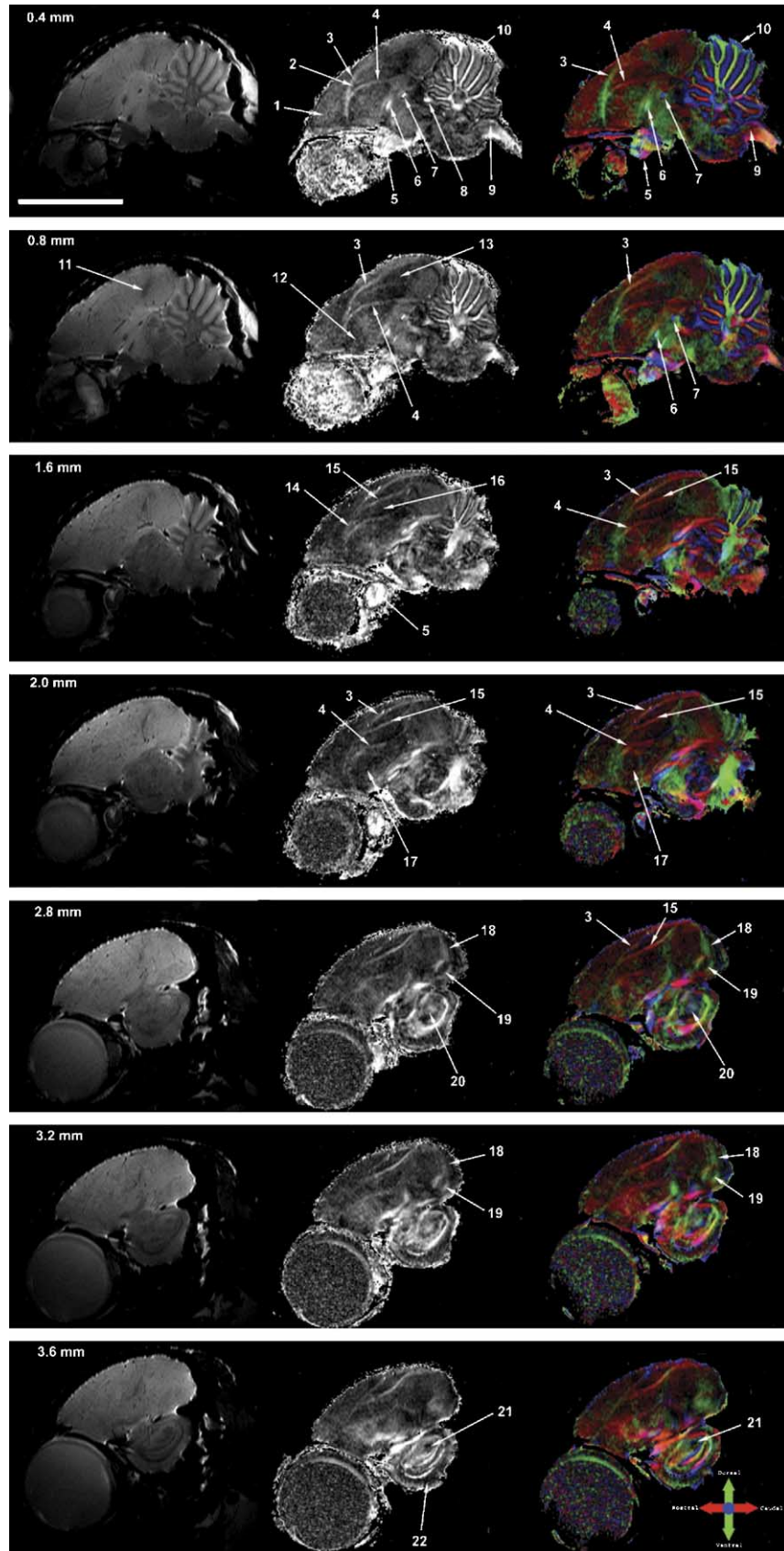


Fig. 3. Coronal Tensor images of in vivo starling brain containing the key song control nuclei HVC, RA and Area X. Two slices (at 4.2 mm Anterior and at 1.8 mm posterior from the reference point of the 1974 Stokes et al. canary brain atlas) are depicted in the three main orthogonal directions (Dxx, Dyy and Dzz). Scale bar = 10 mm.



Dzz). Area X can be seen on all diagonal tensor components but the Dyy component seems to show it more pronounced. RA is clearly visible in the Dxx and Dyy tensor component while RA is less clearly visible in the Dzz component. Tensor maps are based on an internal reference frame (which does not comply with the diffusion frame of the tissue) and thus cannot be used for direct comparison between different measurements and anatomical evaluation.

The DTI parameter maps such as Trace, FA and FEFA are displayed in Fig. 2. Trace maps, obtained simply by summing the diagonal elements of the tensor per voxel, seem to be the least useful maps from a neuroanatomical point of view, as only a few structures can be discerned (Table 2). FA (fractional anisotropy) maps provide per voxel the degree to which the diffusion of water follows one direction, with the brighter the voxel the more ‘cigar shaped’ the diffusion (more anisotropic). A large number of structures can be identified on these maps (Table 2). Each voxel can also be given a color representing the direction of its first eigenvector, and in this way a sense of direction/orientation can be given to the anisotropy of the brain. The latter are called First Eigenvector FA (FEFA) maps. We have chosen to use the FA and FEFA maps for visualization of anatomical structures for the remainder of this study.

In vivo neuroanatomy

Fig. 4 shows three different components obtained from a DTI-experiment from the same sagittal slice: the non-DW image (being a plain T_2 -weighted image) (1st column) and its corresponding FA (2nd column) and FEFA-map (3rd column). It is clear that the (FE)FA-maps display a large amount of brain structures (see caption) not noticeable on plain T_2 -weighted images. Fig. 5 shows FA-maps in a coronal direction illustrating the different laminae, which form the border between different important subdivisions of the telencephalon, like the (3) superior frontal lamina (LFS), the (4) pallial subpallial lamina (LPS), the (15) mesopallial lamina (LaM), the (23) lamina frontalis suprema (LFM) and the (25) lamina arcopallialis dorsalis (LAD). Large telencephalic fiber tracts like the (6) tractus septopallio-mesencephalicus (TSM), the (24) tractus fronto-arcopallialis, the (26) fasciculus prosencephali lateralis or lateral forebrain pathway (FPL) and the (33) Tractus occipito-mesencephalicus (OM) are also easy to distinguish.

The song control system can be divided into two circuits: the motor pathway (caudal circuit) which projects from HVC to the robust nucleus of the arcopallium (RA) and plays a critical role in the production of song and the anterior forebrain pathway or AFP (rostral circuit) which begins with a projection from HVC to area X, a song control nucleus within the basal ganglia which is involved in song learning in juveniles (Bottjer et al., 1984; Scharff and Nottebohm, 1991) and song stability in adults (Brainard and Doupe, 2001). In Fig. 4 (at 2.8 mm from midsagittal), we can discern the HVC-to-X tract running partially

along the Mesopallial lamina (15) and the HVC-to-RA tract (18), the latter is also clearly visible in Fig. 5 (at 1.8 mm posterior from the reference point in the 1974 Stokes atlas). To our knowledge, these tracts have not been visualized in vivo before with any other technique. Other song control nuclei such as medial magnocellular nucleus of anterior nidopallium (MMAN (2)), lateral magnocellular nucleus of anterior nidopallium (LMAN (14)) and even RA (19) surrounded by numerous nerve fibers can also be discerned on the FA maps.

Although HVC itself is the major relay center integrating input from the auditory system and output to RA (19) and X (17), it is not encapsulated by myelinated fibers. Therefore, the nucleus is not easily distinguished on the FA maps. On the coronal maps (Fig. 5), HVC (32) is vaguely seen at 0 to 0.6 mm posterior. Nuclei and structures not related to the song control system, such as the hippocampus (Hp, 28), the anterior and posterior commissures (CoA, 7; CP, 8), some auditory nuclei (nucleus mesencephalicus lateralis, pars dorsalis (MLD (21), Field L2 (11) and several visual system structures (chiasma opticum, (CO (5), nucleus rotundus (Rt (35), tectum opticum (TeO (22) were also discerned. The cerebellum (10) is clearly visible due too the distinct orthogonal organization of its fibers.

DTI fiber tracking

As our primary interest was to visualize the connections between the key song control nuclei, fiber tracking was performed by positioning seed points on the fiber capsule surrounding RA (Figs. 6 and 7). With the dorso-caudal part of the capsule around RA as seed point, the tracking algorithm discriminated fibers representing the HVC-to-RA tract as demonstrated in Fig. 6 in both coronal and sagittal directions. Although it was impossible to know the direction of the fibers traveling between HVC and RA using DTI, it is known from previous studies using tract tracing methods that the neurons have their soma in HVC and project all the way into RA (Mooney and Rao, 1994; Holloway and Clayton, 2001).

All the tracts running to and from RA (or the surrounding arcopallium) became visible (Fig. 7) when the entire capsule around RA was considered as seed point for the tracking algorithm. Usually, the fiber tracts cover more than one slice and provide a three dimensional view of its course. An excellent example is the caudal part of the ‘motor circuit’ of the song control system visualized in Fig. 7, starting at HVC, heading to RA while the next tract starts in RA and goes to the midbrain (via the Tractus occipito-mesencephalicus), in particular to the dorsomedial nucleus of the intercollicular complex (DM) (Nottebohm et al., 1982; Wild et al., 2001). The same figure also illustrates the tract going from the dorsolateral part of the caudal nidopallium (dNCL) to the Dorsal arcopallium (AD), as described earlier by Bottjer et al. (2000). The observation of tracts going to the contralateral telencephalic part of the brain passing through the anterior commissure (CoA) and heading towards the hippocampus corresponds with the suggestion of

Fig. 4. (Left column) T_2 -weighted non-DW image, (middle column) FA-map and (right column) FEFA-map of sagittal sections of the starling brain (0.4 mm from midsagittal – top image – to 3.6 mm – bottom image) obtained in vivo. From top to bottom, the sections are 0.4, 0.8, 1.6, 2.0, 2.8, 3.2 and 3.6 mm lateral to the middle of the brain. The following structures are visible: (1) hyperpallium, (2) medial magnocellular nucleus of anterior nidopallium, (3) lamina frontalis superior, (4) lamina pallio-subpallialis, (5) chiasma opticum, (6) Tractus septopallio-mesencephalicus, (7) commissura anterior, (8) commissura posterior, (9) hypoglossal nucleus, (10) cerebellum, (11) field L2, (12) striatum mediale, (13) mesopallium, (14) lateral magnocellular nucleus of anterior nidopallium, (15) lamina mesopallialis, (16) nidopallium, (17) area X, (18) HVC-to-RA tract, (19) robust nucleus of the arcopallium, (20) nucleus intercollicularis, (21) nucleus mesencephalicus lateralis pars dorsalis, (22) tectum opticum. Scale bar = 10 mm.

Szekely (1999) and Atoji and Wild (2004) that the hippocampus (Hp) has projections towards the dorsal arcopallium (AD).

Discussion

The present data demonstrate that DTI can be used to accurately discern the white matter distribution and the laminae in the avian telencephalon in vivo and non-invasively. Connections, such as the HVC-to-RA tract, which are not seen with any other in vivo technique, were visualized here in vivo for the first time using the DTI technique. The color-coded FEFA-maps provided information on the orientation in which the fibers traverse the brain. An initial analysis with tractography using a color-coded indication of fiber orientation revealed some key fibers, e.g., HVC-to-RA pathway, using RA and surrounding tissue as seeding point. Diffusion Tensor Imaging allows us to visualize more structures than normally seen on T_1 or T_2 weighted images. Using fiber tracking software the following structures can be visualized: parts of the song control system such as RA and area X, the connection between HVC and RA, other connections of the song control system, such as most of the ‘motor circuit’ starting from HVC over RA to DM.

The HVC-RA connection is known to emerge after hatching and during the period of song learning and shows remarkable plasticity in the amount of fibers in adult life (Mooney and Rao, 1994). Therefore, the introduction of DTI in the songbird model will not only allow validation of the accuracy of existing DTI acquisition and processing methods for evaluation of fiber de- and re-generation but will allow the design of new experimental setups in the songbird to explore biological mechanisms involved in brain plasticity.

The DTI experiments performed in this study were preceded by a careful optimization of several image parameters (resolution, slice thickness, b values and number of averages) which ultimately made DTI and fiber tracking in starling brain possible. Because the bird’s skull harbors many small air cavities, the use of ultra fast imaging sequences results in susceptibility distortions unless optimization at the level of hardware (e.g., shims, gradients) and development of correction schemes for the image reconstruction are taken care of. We approached this without these accommodations and designed a setup for validation of DTI in songbirds using a conventional Spin Echo Diffusion Weighted (SE-DW) sequence

(see material and methods). In order to perform DTI in a reasonable timescale for in vivo imaging we used parameters that allowed us to acquire one DTI-dataset within 8 h and thirty min, a time span that allowed 100% complete recovery of the birds. To that end, multi-slice SE-DW imaging with 14 averages per image was used to compensate for the loss in Signal to Noise. The use of a multi-slice setup also led in this case to datasets with non-isotropic voxels ($400 \mu\text{m}$ in slice direction and $98 \times 98 \mu\text{m}^2$ in plane). Although in this study a minimum of seven non-collinear directions was used, the high magnetic field strength of 7 T and the high resolution of $100 \mu\text{m}$ allowed us to track fibers accurately.

It is not entirely clear which aspects of the neuron/axon give rise to anisotropy and to what extent crossing fibers in one voxel affect the accuracy of the fiber tracking. Fiber tracking in the highly

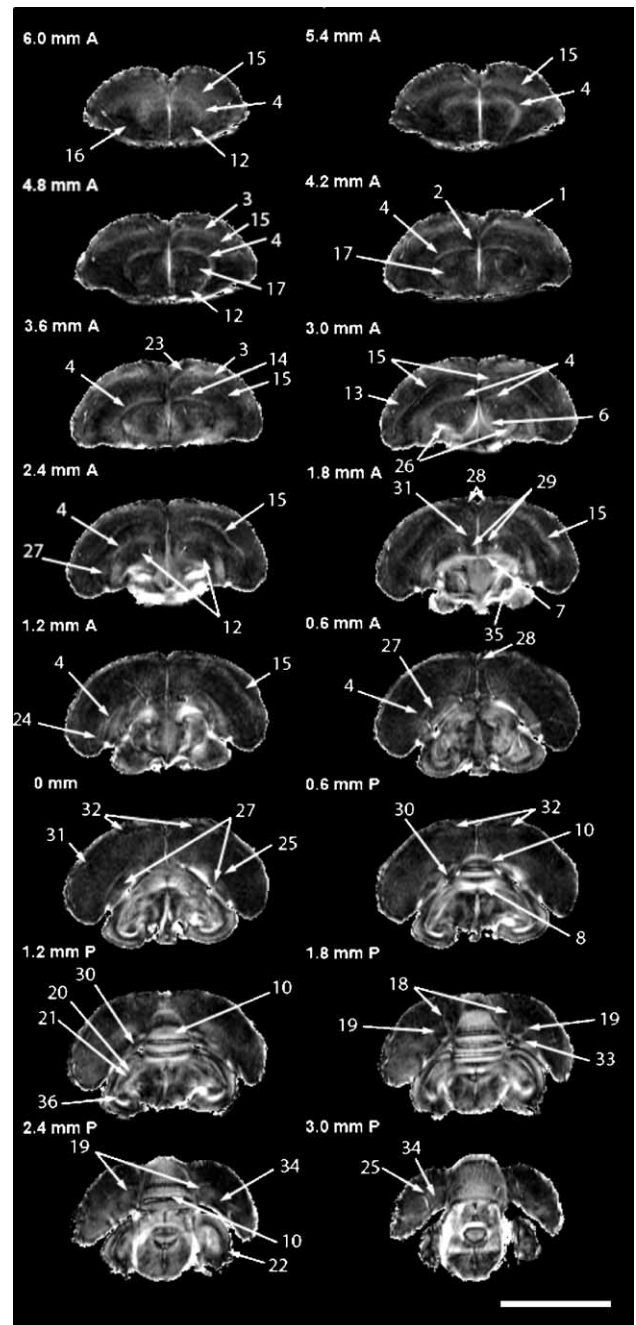


Fig. 5. FA-maps (coronal sections) of starling brain in vivo. Starting top left, going to top right and then further down same way sections are displayed from 6.0 mm anterior to 3 mm posterior from the 1974 Stokes et al. atlas reference point, with slice thickness of 0.6 mm. The following structures are visible: (1) hyperpallium, (2) medial magnocellular nucleus of anterior nidopallium, (3) lamina frontalis superior, (4) lamina pallio-subpallialis, (5) chiasma opticum not seen on these slices, (6) tractus septopallio-mesencephalicus, (7) commissura anterior, (8) commissura posterior, (9) hypoglossal nucleus not seen on these slices, (10) cerebellum, (11) field L2, not seen on these slices, (12) striatum mediale, (13) mesopallium, (14) lateral magnocellular nucleus of anterior nidopallium, (15) lamina mesopallialis, (16) nidopallium, (17) area X, (18) HVC-to-RA tract, (19) robust nucleus of the arcopallium, (20) nucleus intercollicularis, (21) nucleus mesencephalicus lateralis pars dorsalis, (22) tectum opticum, (23) lamina frontalis suprema, (24) tractus fronto-arcopallialis, (25) lamina arcopallialis dorsalis, (26) fasciculus prosencephali lateralis or lateral forebrain pathway, (27) striatum laterale, (28) hippocampus, (29) nucleus septalis medialis, (30) nucleus taenia amygdale, (31) ventricle, (32) HVC, (33) tractus occipito-mesencephalicus, (34) arcopallium, (35) nucleus rotundus, (36) nucleus isthmi. Scale bar = 10 mm.

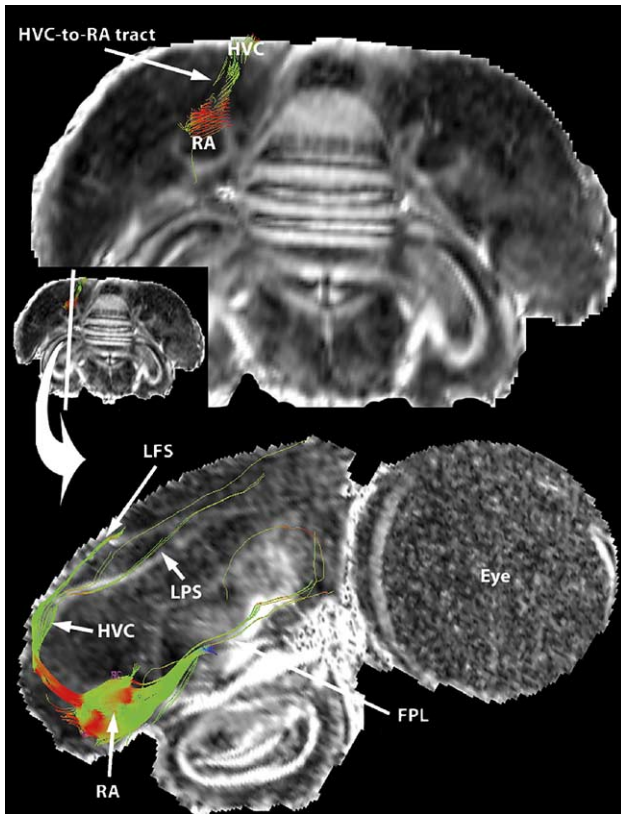


Fig. 6. (top) FA-maps with projected fibers of a coronal slice taken 1.8 mm posterior from the 1974 Stokes et al. atlas reference point, with seed point chosen at the top of RA. (bottom) FA-maps with projected fibers of a sagittal slice taken 2.8 mm from midsagittal with seed point chosen around RA from two slices (2.8 and 3.2 mm from midsagittal). Color code of the fibers on the coronal slice is according to orientation; red = medial ↔ lateral orientation, green = dorsal ↔ ventral orientation, blue = rostral ↔ caudal orientation. Sagittal slice: red = dorsal ↔ ventral orientation, green = rostral ↔ caudal orientation, blue = medial ↔ lateral orientation. Abbreviations: RA: robust nucleus of the arcopallium; LPS: lamina pallio-subpallialis; LFS: lamina frontalis superior; FPL: fasciculus prosencephali lateralis or lateral forebrain pathway. Because of the 3D nature of the tracts, they extend to more slices than the one shown here.

plastic HVC-RA connection might provide insight into the different physiological contributions to the diffusion contrast on which the tracking algorithms are based. Songbirds also make an interesting model for DT fiber tracking because the entire brain seems to consist of grey matter with very distinct white matter tracts that are, within the telencephalon, largely organized in laminae.

Anisotropic water diffusion is in most of the visualized fiber tracts undoubtedly related to the ordered arrangement of myelinated fibers in nerves and white matter, but myelin is not the sole source of anisotropy. Beaulieu and Allen (1994) proved this by showing that water diffusion was significantly anisotropic in a normal, intact non-myelinated olfactory nerve of the garfish. This is not to say that myelin does not play a role in anisotropy, but rather this observation serves to point out structural features of the axons (the axonal membrane, axonal transport, neurofibrils) other than myelin are sufficient to give rise to anisotropy and that interpretation of changes in anisotropy with respect to myelination only must be made with caution. (for a full technical review on this matter, see Beaulieu, 2002).

It should also be pointed out that the FA value of a voxel needs to attain a certain FA threshold in order to be incorporated into a ‘fiber’. The FA value increases exponentially when more (un)myelinated axons are present (and aligned in one direction) in one voxel, so a minimum number of axons is needed for the tracking algorithm to work. Therefore, one fiber generated with the fiber tracking algorithm does not represent a single axon, but at least 50 of them (mean axon diameter for birds is $\pm 2 \mu\text{m}$). Only larger fiber bundles, such as the HVC-to-RA tract, can be visualized using DT-fiber tracking. This brings us to another drawback of fiber tracking, namely the ‘crossing fibers problem’. Because of the voxel-averaged nature of diffusion tensor, only the superimposed averaged diffusion direction of all fiber structures inside a voxel is dominant. Consequently, tracking algorithms are not adequate for regions with crossing fiber pathways and often fail in such situations. This is a key obstacle for fiber tractography based on DTI data.

Although there are obvious differences between the brains of birds and mammals, songbirds could be considered a good model for the developing brain and the formation of white matter tracts. Similar to humans, songbirds do not have a fully developed brain when they hatch (Arnold, 1992). As a young child learns how to speak, so juvenile songbirds learn how to sing and communicate, a trait not found in many animals (Doupe and Kuhl, 1999; Wilbrecht and Nottebohm, 2003). The white matter tracts in the cerebral hemispheres of the premature human brain are unmyelinated, except for a few early-maturing pathways such as the pyramidal tract as the baby approaches 37th week of gestation (Kinney et al., 1988, 1994). Structural maturation of fiber tracts in the human brain, including an increase in the diameter and myelination of axons, may play a role in cognitive development during childhood and adolescence. Paus et al. (1999) showed evidence that during late childhood and adolescence the fiber pathways supporting speech functions gradually mature. The songbird brain probably

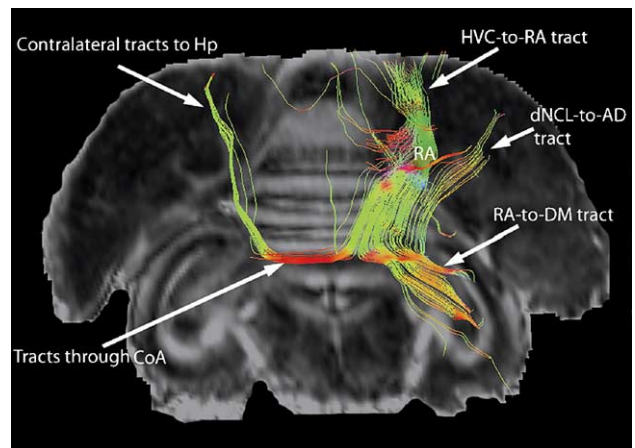


Fig. 7. FA-map with projected fibers of a coronal slice taken 1.8 mm posterior from the 1974 Stokes et al. atlas reference point, with the seed point chosen around RA. Abbreviations: AD: dorsal arcopallium; CoA: commissura anterior; DM: dorsomedial nucleus of the intercollicular complex; dNCL: dorsolateral caudal nidopallium; Hp: hippocampus; RA: robust nucleus of the arcopallium. Color code of the fibers is according to orientation; red = medial ↔ lateral orientation, green = dorsal ↔ ventral orientation, blue = rostral ↔ caudal orientation. Because of the 3D nature of the tracts, they extend to more slices than the one shown here, e.g., Hp, HVC, dNCL, CoA and DM are not seen on this slice.

shows the same process of developing white matter tracts during early ontogeny (Arnold, 1992). Diffusion Tensor Imaging has been used in many studies of the developing human brain (Rivkin, 2000; Neil et al., 2002; McKinstry et al., 2002; Mukherjee et al., 2002; Maas et al., 2004; Partridge et al., 2004), but it can take several years for a longitudinal study of childhood development. Similar studies could be performed in songbirds, following individual birds from egg to adulthood, in a much shorter time span. Another reason why songbirds should be meticulously investigated is because the formation of white matter tracts doesn't stop when songbirds become adults; unlike most animals many songbirds show a seasonal neuroplasticity during their lifetime (Ball et al., 2004; Brenowitz, 2004) making them an ideal model for neuroplasticity studies. DTI could be considered a very valuable tool for investigating seasonal changes in the structure and connections of the song control nuclei, and this perhaps as a complementary tool to Manganese Enhanced MRI (MEMRI) (Van Meir et al., 2004).

As this study has shown, DTI is an excellent tool for in vivo neuroanatomy of the songbird brain. However, another interesting application could be the combined use with functional MRI (fMRI). fMRI allows the in vivo mapping of activated brain regions (Van Meir et al., 2005). Fiber tracking could provide complementary information, by showing the connections that allow these activated areas to communicate with each other.

DTI of the songbird brain displays great potential in providing specific non-invasive and in vivo information in the quest for unraveling the structure and function of the song control system, and other neural circuits in the songbird brain.

Acknowledgments

We are grateful to Dr. J. Martin Wild (University of Auckland, Auckland, New Zealand) for critical review of anatomical structure assignment.

This research was supported by grants from the National Science Foundation (FWO, project No. G.0420.02) and BOF-NOI and RAFO and GOA funds from the University of Antwerp to AVdL. VVM, IT and AL are grant holders from the Institute for the Promotion of Innovation by Science and Technology in Flanders (IWT-V).

References

- Aamodt, S.M., Kozlowski, M.R., Nordeen, E.J., Nordeen, K.W., 1992. Distribution and developmental change in [3H]MK-801 binding within zebra finch song nuclei. *J. Neurobiol.* 23, 997–1005.
- Ahlhelm, F., Hagen, T., Schneider, G., Dorenbeck, U., Nabhan, A., Reith, W., 2004. ADC mapping of normal human brain. *Med. Sci. Monit.* 10, MT121–MT125.
- Arnold, A.P., 1992. Developmental plasticity in neural circuits controlling birdsong: sexual differentiation and the neural basis of learning. *J. Neurobiol.* 23, 1506–1528.
- Atoji, Y., Wild, J.M., 2004. Fiber connections of the hippocampal formation and septum and subdivisions of the hippocampal formation in the pigeon as revealed by tract tracing and kainic acid lesions. *J. Comp. Neurol.* 475 (3), 426–461 (Jul 26).
- Ball, G.F., Auger, C.J., Bernard, D.J., Charlier, T.D., Sartor, J.J., Ritters, L.V., Balthazart, J., 2004. Seasonal plasticity in the song control system: multiple brain sites of steroid hormone action and the importance of variation in song behavior. *Ann. N. Y. Acad. Sci.* 1016, 586–610.
- Beaulieu, C., 2002. The basis of anisotropic water diffusion in the nervous system—A technical review. *NMR Biomed.* 15, 435–455.
- Beaulieu, C., Allen, P.S., 1994. Water diffusion in the giant axon of the squid: implications for diffusion-weighted MRI of the nervous system. *Magn. Reson. Med.* 32, 579–583.
- Bottjer, S.W., Miesner, E.A., Arnold, A.P., 1984. Forebrain lesions disrupt development but not maintenance of song in passerine birds. *Science* 224, 901–903.
- Bottjer, S.W., Brady, J.D., Cribbs, B., 2000. Connections of a motor cortical region in zebra finches: relation to pathways for vocal learning. *J. Comp. Neurol.* 420, 244–260.
- Brainard, M.S., Doupe, A.J., 2001. Postlearning consolidation of birdsong: stabilizing effects of age and anterior forebrain lesions. *J. Neurosci.* 21, 2501–2517.
- Brenowitz, E.A., 2004. Plasticity of the adult avian song control system. *Ann. N. Y. Acad. Sci.* 1016, 560–585.
- Del Negro, C., Edeline, J.M., 2001. Differences in auditory and physiological properties of HVC neurons between reproductively active male and female canaries (*Serinus canaria*). *Eur. J. Neurosci.* 14, 1377–1389.
- Doupe, A.J., Kuhl, P.K., 1999. Birdsong and human speech: common themes and mechanisms. *Annu. Rev. Neurosci.* 22, 567–631.
- Gaser, C., Schlaug, G., 2003. Gray matter differences between musicians and nonmusicians. *Ann. N. Y. Acad. Sci.* 999, 514–517.
- Holloway, C.C., Clayton, D.E., 2001. Estrogen synthesis in the male brain triggers development of the avian song control pathway in vitro. *Nat. Neurosci.* 4, 170–175.
- Jarvis, E.D., Gunturkun, O., Bruce, L., Csillag, A., Karten, H., Kuenzel, W., Medina, L., Paxinos, G., Perkel, D.J., Shimizu, T., Striedter, G., Wild, J.M., Ball, G.F., Dugas-Ford, J., Durand, S.E., Hough, G.E., Husband, S., Kubikova, L., Lee, D.W., Mello, C.V., Powers, A., Siang, C., Smulders, T.V., Wada, K., White, S.A., Yamamoto, K., Yu, J., Reiner, A., Butler, A.B., 2005. Avian brains and a new understanding of vertebrate brain evolution. *Nat. Rev. Neurosci.* 6, 151–159.
- Kim, D.S., Kim, M., Ronen, I., Formisano, E., Kim, K.H., Ugurbil, K., Mori, S., Goebel, R., 2003. In vivo mapping of functional domains and axonal connectivity in cat visual cortex using magnetic resonance imaging. *Magn. Reson. Imaging* 21, 1131–1140.
- Kinney, H.C., Brody, B.A., Kloman, A.S., Gilles, F.H., 1988. Sequence of central nervous system myelination in human infancy: II. Patterns of myelination in autopsied infants. *J. Neuropathol. Exp. Neurol.* 47, 217–234.
- Kinney, H.C., Karthigasan, J., Borenshteyn, N.I., Flax, J.D., Kirschner, D.A., 1994. Myelination in the developing human brain: biochemical correlates. *Neurochem. Res.* 19, 983–996.
- Le Bihan, D., Mangin, J.F., Poupon, C., Clark, C.A., Pappata, S., Molko, N., Chabriet, H., 2001. Diffusion tensor imaging: concepts and applications. *J. Magn. Reson. Imaging* 13, 534–546.
- Leemans, A., Sijbers, J., Verhoye, M., Van der Linden, A., Van Dyck, D., 2005a. Mathematical framework for simulating diffusion tensor MR neural fiber bundles. *Magn. Reson. Med.* 53, 944–953.
- Leemans, A., Sijbers, J., Parizel, P., 2005b. A Graphical Toolbox for Exploratory Diffusion Tensor Imaging and Fiber Tractography, Section for Magnetic Resonance Technologists (SMRT). 14th Annual Meeting in Miami Beach, Florida, USA.
- Lin, C.P., Tseng, W.Y., Cheng, H.C., Chen, J.H., 2001. Validation of diffusion tensor magnetic resonance axonal fiber imaging with registered manganese-enhanced optic tracts. *NeuroImage* 14, 1035–1047.
- Maas, L.C., Mukherjee, P., Carballido-Gamio, J., Veeraraghavan, S., Miller, S.P., Partridge, S.C., Henry, R.G., Barkovich, A.J., Vigneron, D.B., 2004. Early laminar organization of the human cerebrum demonstrated with diffusion tensor imaging in extremely premature infants. *NeuroImage* 22, 1134–1140.
- Maes, F., Collignon, A., Vandermeulen, D., Marchal, G., Suetens, P., 1997. Multimodality image registration by maximization of mutual information. *IEEE Trans. Med. Imag.* 16, 187–198.
- Maguire, E.A., Gadian, D.G., Johnsrude, I.S., Good, C.D., Ashburner, J.,

- Frackowiak, R.S., Frith, C.D., 2000. Navigation-related structural change in the hippocampi of taxi drivers. *Proc. Natl. Acad. Sci. U. S. A.* 97, 4398–4403.
- Mattiello, J., Basser, P.J., Le Bihan, D., 1997. The b matrix in diffusion tensor echo-planar imaging. *Magn. Reson. Med.* 37, 292–300.
- McKinstry, R.C., Mathur, A., Miller, J.H., Ozcan, A., Snyder, A.Z., Scheff, G.L., Almli, C.R., Shiran, S.I., Conturo, T.E., Neil, J.J., 2002. Radial organization of developing preterm human cerebral cortex revealed by non-invasive water diffusion anisotropy MRI. *Cereb. Cortex* 12, 1237–1243.
- Mooney, R., Rao, M., 1994. Waiting periods versus early innervation: the development of axonal connections in the zebra finch song system. *J. Neurosci.* 14, 6532–6543.
- Mori, S., Barker, P.B., 1999. Diffusion magnetic resonance imaging: its principle and applications. *Anat. Rec.* 257, 102–109.
- Mori, S., Crain, B.J., Chacko, V.P., van Zijl, P.C.M., 1999. Three-dimensional tracking of axonal projections in the brain by magnetic resonance imaging. *Ann. Neurol.* 45, 265–269.
- Moseley, M.E., Cohen, Y., Kucharczyk, J., Mintorovitch, J., Asgari, H.S., Wendland, M.F., Tsuruda, J., Norman, D., 1990. Diffusion-weighted MR imaging of anisotropic water diffusion in cat central nervous system. *Radiology* 176, 439–445.
- Mukherjee, P., Miller, J.H., Shimony, J.S., Philip, J.V., Nehra, D., Snyder, A.Z., Conturo, T.E., Neil, J.J., McKinstry, R.C., 2002. Diffusion-tensor MR imaging of gray and white matter development during normal human brain maturation. *Am. J. Neuroradiol.* 23, 1445–1456.
- Neil, J., Miller, J., Mukherjee, P., Huppi, P.S., 2002. Diffusion tensor imaging of normal and injured developing human brain—A technical review. *NMR Biomed.* 15, 543–552.
- Nottebohm, F., Kelley, D.B., Paton, J.A., 1982. Connections of vocal control nuclei in the canary telencephalon. *J. Comp. Neurol.* 207, 344–357.
- Partridge, S.C., Mukherjee, P., Henry, R.G., Miller, S.P., Berman, J.I., Jin, H., Lu, Y., Glenn, O.A., Ferriero, D.M., Barkovich, A.J., Vigneron, D.B., 2004. Diffusion tensor imaging: serial quantitation of white matter tract maturity in premature newborns. *NeuroImage* 22, 1302–1314.
- Paus, T., Zijdenbos, A., Worsley, K., Collins, D.L., Blumenthal, J., Giedd, J.N., Rapoport, J.L., Evans, A.C., 1999. Structural maturation of neural pathways in children and adolescents: in vivo study. *Science* 283, 1908–1911.
- Reiner, A., Perkel, D.J., Bruce, L.L., Butler, A.B., Csillag, A., Kuenzel, W., Medina, L., Paxinos, G., Shimizu, T., Striedter, G., Wild, M., Ball, G.F., Durand, S., Gutarun, O., Lee, D.W., Mello, C.V., Powers, A., White, S.A., Hough, G., Kubikova, L., Smulders, T.V., Wada, K., Dugas, F., Husband, S., Yamamoto, K., Yu, J., Siang, C., Jarvis, E.D., 2004. Revised nomenclature for avian telencephalon and some related brainstem nuclei. *J. Comp. Neurol.* 473, 377–414.
- Riters, L.V., Ball, G.F., 2002. Sex differences in the densities of alpha(2)-adrenergic receptors in the song control system, but not the medial preoptic nucleus in zebra finches. *J. Chem. Neuroanat.* 23, 269–277.
- Rivkin, M.J., 2000. Developmental neuroimaging of children using magnetic resonance techniques. *Ment. Retard. Dev. Disabil. Res. Rev.* 6, 68–80.
- Ronen, I., Kim, K.H., Garwood, M., Ugurbil, K., Kim, D.S., 2003. Conventional DTI vs. slow and fast diffusion tensors in cat visual cortex. *Magn. Reson. Med.* 49, 785–790.
- Scharff, C., Nottebohm, F., 1991. A comparative study of the behavioral deficits following lesions of various parts of the zebra finch song system: implications for vocal learning. *J. Neurosci.* 11, 2896–2913.
- Sohrabji, F., Nordeen, E.J., Nordeen, K.W., 1990. Selective impairment of song learning following lesions of a forebrain nucleus in the juvenile zebra finch. *Behav. Neural Biol.* 53, 51–63.
- Song, S.K., Sun, S.W., Ramsbottom, M.J., Chang, C., Russell, J., Cross, A.H., 2002. Demyelination revealed through MRI as increased radial (but unchanged axial) diffusion of water. *NeuroImage* 17, 1429–1436.
- Song, S.K., Sun, S.W., Ju, W.K., Lin, S.J., Cross, A.H., Neufeld, A.H., 2003. Diffusion tensor imaging detects and differentiates axon and myelin degeneration in mouse optic nerve after retinal ischemia. *NeuroImage* 20, 1714–1722.
- Song, S.K., Kim, J.H., Lin, S.J., Brendza, R.P., Holtzman, D.M., 2004. Diffusion tensor imaging detects age-dependent white matter changes in a transgenic mouse model with amyloid deposition. *Neurobiol. Dis.* 15, 640–647.
- Stejskal, E., Tanner, J., 1965. Spin diffusion measurements: spin echoes in the presence of a time dependent field gradient. *J. Chem. Phys.* 42, 288–292.
- Stokes, T.M., Leonard, C.M., Nottebohm, F., 1974. The telencephalon, diencephalon, and mesencephalon of the canary, *Serinus canaria*, in stereotaxic coordinates. *J. Comp. Neurol.* 156, 337–374.
- Sun, S.W., Song, S.K., Hong, C.Y., Chu, W.C., Chang, C., 2003. Directional correlation characterization and classification of white matter tracts. *Magn. Reson. Med.* 49, 271–275.
- Szekely, A.D., 1999. The avian hippocampal formation: subdivisions and connectivity. *Behav. Brain Res.* 98, 219–225.
- Thompson, C.K., Brenowitz, E.A., 2005. Seasonal change in neuron size and spacing but not neuronal recruitment in a basal ganglia nucleus in the avian song control system. *J. Comp. Neurol.* 481, 276–283.
- Tindemans, I., Verhoye, M., Balthazart, J., Van der Linden, A., 2003. In vivo dynamic ME-MRI reveals differential functional responses of RA- and area X-projecting neurons in the HVC of canaries exposed to conspecific song. *Eur. J. Neurosci.* 18, 3352–3360.
- Tramontin, A.D., Brenowitz, E.A., 2000. Seasonal plasticity in the adult brain. *Trends Neurosci.* 23, 251–258.
- Tramontin, A.D., Smith, G.T., Breuner, C.W., Brenowitz, E.A., 1998. Seasonal plasticity and sexual dimorphism in the avian song control system: stereological measurement of neuron density and number. *J. Comp. Neurol.* 396, 186–192.
- Van der Linden, A., Verhoye, M., Peeters, R., Eens, M., Newman, S.W., Smulders, T., Balthazart, J., DeVoogd, T.J., 1998. Non invasive in vivo anatomical studies of the oscine brain by high resolution MRI microscopy. *J. Neurosci. Methods* 81, 45–52.
- Van der Linden, A., Verhoye, M., Van Meir, V., Tindemans, I., Eens, M., Absil, P., Balthazart, J., 2002. In vivo manganese-enhanced magnetic resonance imaging reveals connections and functional properties of the songbird vocal control system. *Neuroscience* 112, 467–474.
- Van der Linden, A., Van Meir, V., Tindemans, I., Verhoye, M., Balthazar, J., 2004. Applications of manganese-enhanced magnetic resonance imaging (MEMRI) to image brain plasticity in song birds. *NMR Biomed.* 17, 602–612.
- Van Meir, V., Verhoye, M., Absil, P., Eens, M., Balthazar, J., Van der Linden, A., 2004. Differential effects of testosterone on neuronal populations and their connections in a sensorimotor brain nucleus controlling song production in songbirds: a manganese enhanced-magnetic resonance imaging study. *NeuroImage* 21, 914–923.
- Van Meir, V., Boumans, T., De Groof, G., Van Audekerke, J., Smolders, A., Scheunders, P., Sijbers, J., Verhoye, M., Balthazart, J., Van der Linden, A., 2005. Spatiotemporal properties of the BOLD response in the songbirds' auditory circuit during a variety of listening tasks. *NeuroImage* 25, 1242–1255.
- Verhoye, M., Van der Linden, A., Van Audekerke, J., Sijbers, J., Eens, M., Balthazart, J., 1998. Imaging birds in a bird cage: in-vivo FSE 3D MRI of bird brain. *MAGMA* 6, 22–27.
- Wilbrecht, L., Nottebohm, F., 2003. Vocal learning in birds and humans. *Ment. Retard. Dev. Disabil. Res. Rev.* 9, 135–148.
- Wild, J.M., Williams, M.N., Suthers, R.A., 2001. Parvalbumin-positive projection neurons characterise the vocal premotor pathway in male, but not female, zebra finches. *Brain Res.* 917, 235–252.
- Xue, R., van Zijl, P.C., Crain, B.J., Solaiyappan, M., Mori, S., 1999. In vivo three-dimensional reconstruction of rat brain axonal projections by diffusion tensor imaging. *Magn. Reson. Med.* 42, 1123–1127.
- Yamazaki, Y., Murase, K., Kumashiro, M., Okamoto, E., Obara, M., Van Cauteren, M., Watanabe, Y., 2004. Three-dimensional Visualization of White Matter Fibers and Tissue Structures Using Diffusion Tensor Magnetic Resonance Imaging of the Brain. *Medinfo*, p. 1918.
- Zhang, J., van Zijl, P.C., Mori, S., 2002. Three-dimensional diffusion tensor magnetic resonance microimaging of adult mouse brain and hippocampus. *NeuroImage* 15, 892–901.